

Effects of space weather on the ionosphere: A case study of geomagnetic storms during 17-28 February 2014

Sharon Aol*, Patrick Mungufeni and Edward Jurua
Mbarara University of Science and Technology, Uganda

Received 9 November 2017; accepted 4 October 2019

This study focused on the effects of space weather on the ionosphere during geomagnetic storms for the period 17-28 February 2014 over the African low, latitude region. The Global Positioning System (GPS) data, derived from dual frequency receivers installed along the African low, latitude were analyzed to get Total Electron Content (TEC) and this was used to study the response of the ionosphere to the geomagnetic storms. Positive and negative ionospheric storm effects were observed during the period of study. These geomagnetic storm effects were discussed in terms of the Prompt Penetration Electric Field (PPEF) storm induced wind lifting effect and Disturbance Dynamo (DD) electric field. Although these storms occurred during the same period, their impacts and associated features on the ionosphere varied due to different contributing factors to their driving mechanisms. A shift in equatorial *VTEC* enhancement from one GPS station to another was observed, showing a longitudinal dependence of the ionospheric response to the geomagnetic storms and this was attributed to composition changes. In addition, Rate of Change of TEC Index (*ROTI*) was used to examine the occurrence of ionospheric irregularities. Out of all the storms studied, the storms on 19 and 20 February 2014, inhibited the occurrence of ionospheric irregularities, while the remaining storms triggered ionospheric irregularities. The generation of post-sunset irregularities was attributed to the Rayleigh Taylor Instability mechanism. A longitudinal dependence of the enhancement/inhibition of ionospheric irregularities was also observed.

Keywords: Space weather, Geomagnetic storms, Ionospheric disturbances

1 Introduction

In an ideal situation, the Earth's magnetic field has a fairly uniform dipole configuration, but an encounter with fast-moving solar wind results into its significant disturbance¹⁻³. These disturbances that affect the entire magnetosphere-ionosphere coupled system are called geomagnetic storms. The dominant interplanetary structures associated with geomagnetic disturbance causing intense storms are the interplanetary manifestation of coronal mass ejections (CMEs) and high-speed solar wind stream (CIRs mechanism)⁴. The CME is a large scale magnetized plasma structure originating from the Sun which is ejected into the interplanetary medium through the solar corona. The CIRs develop when fast streams originating from the coronal holes interact with the slow solar wind. These compress the magnetic field and the plasma ahead and sometimes, though not always, creating a shock front, which is the cause of recurrent geomagnetic storms⁵. Geomagnetic storms are caused by strong dawn-to-dusk electrical fields linked to the passage of the

southward Interplanetary Magnetic Field (IMF Bz)¹. The energy transfer from the solar wind is through magnetic re-connection between the IMF Bz and the Earth's magnetic field. During magnetic reconnection, energy is injected into the upper atmosphere at auroral regions through particle precipitation and ionospheric plasma convection which leads to an increase in the auroral current. The auroral electric currents transfer energy to the neutral gas via Joule heating and they also move the neutral wind via momentum transfer. Joule heating and momentum force drive thermospheric winds and pressure at F-region heights. The thermospheric winds extend towards the middle and low-latitudes. These winds also lift the ionization to regions of lower loss, producing a day time increase in ionospheric parameters and global changes in atmospheric composition⁶⁻¹⁰. The electron density of the ionosphere is highly sensitive to this energy transfer and it may fluctuate from its quiet time value thereby affecting communication and navigation systems which rely on satellite technology^{11,12}.

The electron density fluctuations in the ionosphere arising during the period of active geomagnetic activity are linked to the complex electrodynamic changes in

*Corresponding author (Email: sharonaol@ymail.com)

the ionosphere¹³. The effects of storm time electrodynamic, neutral winds and subsequent changes in composition have revealed an increase or decrease in the ionospheric F-region density, e.g.¹⁴, referred to as positive and negative ionospheric storms respectively¹³. Previous studies of electrodynamic changes in the ionosphere due to geomagnetic storms have revealed the occurrence of large electric fields and currents during and after geomagnetically disturbed periods e.g.¹⁵. The electric fields have been identified as the Prompt Penetration Electric Field (PPEF) and the Disturbance Dynamo (DD) electric field. The PPEF is transmitted to the mid and low latitudes on the time scales of an hour or so e.g.¹⁶. The time scales associated with the transmission of the DD electric fields are much longer e.g.¹⁷. The two electric fields are oppositely directed at the equator with the DD electric field being westward during day and eastward in the night¹⁸, whereas the direction of the zonal ambient electric field is eastward during daytime and westward in the night.

During geomagnetic storms, strong eastward (westward) electric fields originating from the magnetosphere may penetrate to the mid and low latitude ionosphere. This may lead to the intensification (weakening) of the upward plasma $\vec{E} \times \vec{B}$ drift^{19,20}. Hence, the disturbance fields produce remarkable effects in the low latitude ionosphere due to the modification of the $\vec{E} \times \vec{B}$ vertical plasma drift. As a result, the fountain effect may be modified considerably, leading to redistribution of plasma in the anomaly zone latitudes. The DD electric fields are produced due to the increase in radiation and consequent Joule heating of the high latitude plasma²¹⁻²² added that this additional heating may launch winds towards the equator, which in turn generate DD electric fields. The DD effect makes the equatorial F-region plasma drift less upwards during the day and less downwards in the night²².

Enormous work has been done to understand ionospheric dynamics during geomagnetic storms at all latitudes e.g.^{3,11-15,18,22-28}. Some of these studies have presented results on the geomagnetic storms which occurred during 17-28 February 2014 e.g.²⁹⁻³² investigated geomagnetic pulsations, Ultra Low Frequency (ULF) waves during this period. A non-sub storm Pi2 pulsation was observed on 26 February 2018 with nearly identical wave forms and a Pc4 pulsation was also observed on the recovery phase of the storm on 23 February 2014³⁰

explored the ionospheric and thermospheric responses to the 27-28 February 2014 geomagnetic storms over North Africa using interferometer, all-sky imager and GPS data. Traveling atmospheric disturbances were evident in the meridional winds, the first one coming from the northern hemisphere and the second one coming from the southern hemisphere. The VTEC response of the storm was positive and TIDs were noticeable from the TEC pattern³² presented observations of equatorial plasma bubbles in the topside ionosphere at early morning hours (05-08 LT) in the recovery phase of the 18-19 February 2014 geomagnetic storm. However, it is not yet possible to accurately forecast the response of the ionosphere to geomagnetic storms²⁶ due to the fact that every geomagnetic storm possesses a distinct character^{14,25,27,33}. The distribution of ionospheric storm effects may vary highly from one geomagnetic storm event to another^{23,27}. Until a complete understanding of the processes that lead to an ionospheric storm develops, variations in TEC during each storm requires to be investigated in real time to mitigate the errors in GPS navigation³⁴.

The period 17-28 February 2014 was an active period characterized by a series of CMEs as recorded in the Large Angle and Spectrometric Coronagraph (LASCO) catalogue (cdaw.gsfc.nasa.gov/). In this paper, we contribute to the study of the geomagnetic storms during 17-28 February 2014 by analyzing the signatures of the storms on TEC over the African low latitude region.

2 Data Sources

To analyze the solar wind conditions during the period of study, solar wind parameters were utilized and these included, the IMF Bz, proton speed V_p , solar wind proton temperature T_p and pressure P_{sw} . These parameters were obtained from the Advanced Composition Explorer (ACE) website <http://www.srl.caltech.edu/ACE/ASC/level2>. The Geophysical conditions were represented by the geomagnetic perturbation indices: Auroral Electrojet (AE), Disturbance storm time (Dst) and Kp indices obtained from the Kyoto website <http://wdc.kugi.kyoto-u.ac.jp/dst/dir/>. The AE index is designed to give a global, quantitative measure of auroral zone magnetic activity produced by enhanced ionospheric currents flowing below and within the auroral oval³⁵. The Dst index reflects the level of magnetospheric energy input to the upper atmosphere while the Kp

index provides information on the average level of magnetic activity on a worldwide basis³⁶.

The GPS-derived TEC data were utilized to assess the impact of geomagnetic storms on the ionosphere over the African low latitude region. The TEC data were obtained for the International GNSS Services (IGS) receivers: Libreville (NKLK), Mbarara (MBAR), Eldoret (MOIU), Malindi (MAL2) and Seychelles Island (SEY1), presented in Fig. 1 as red diamonds. The blue lines in Fig.1 represent the ionization anomaly belts which are at $\approx \pm 15^\circ$ on either sides of the geomagnetic equator (red line). The details of the IGS stations used in this study are summarized in Table 1. The GPS data recorded in compact Receiver Independent Exchange (RINEX) format were downloaded from the IGS website <http://garner.ucsd.edu/pub/rinex/> for each receiver. The methods used in analyzing the data are presented here.

3 Methods of Data Analysis

The processing of GPS data was done using the GPS-TEC application software³⁷. The software

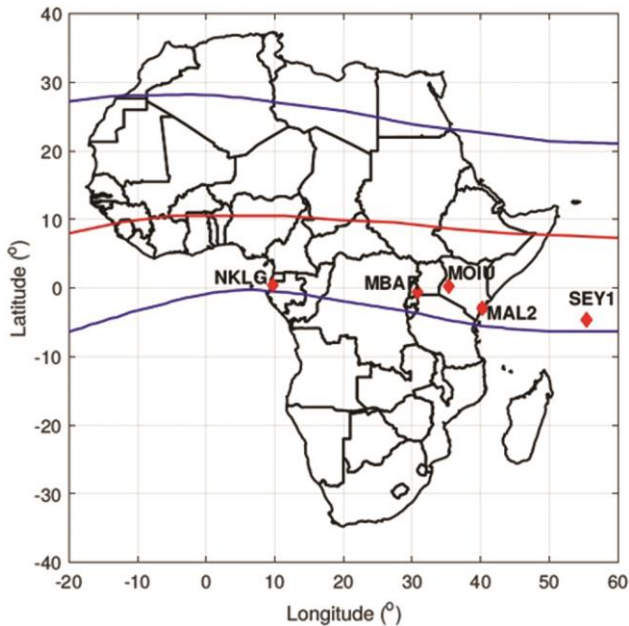


Fig. 1 — African map showing the geographic location of IGS receivers (red diamonds). The ionization anomaly region is represented by blue lines and the geomagnetic equator is represented by red line.

converts the estimated Slant Total Electron Content (*STEC*) with a time resolution of 30 seconds to Vertical Total Electron Content (*VTEC*) according to the equation³⁸:

$$VTEC = \frac{STEC - [b_R \pm b_S]}{S(E_l)} \quad \dots (1)$$

where, b_R and b_S are the receiver and satellite biases respectively, E_l is the elevation angle of the satellite and $S(E_l)$ is the obliquity factor or mapping function with zenith angle z at the Ionospheric Pierce Point (IPP). The satellite biases are published by the University of Bern (<ftp://ftp.unibe.ch/aiub/CODE/>). The $S(E_l)$ is given by the equation³⁹:

$$S(E_l) = \frac{1}{\cos(z)} = \left\{ 1 - \left(\frac{R_E \cos(E_l)}{R_E + H} \right)^2 \right\}^{-\frac{1}{2}} \quad \dots (2)$$

where, $R_E = 6371\text{km}$ is the mean Earth radius and $H = 350\text{km}$ is the height of the ionospheric shell above the earth's surface. Only satellite for which the elevation angle was $\geq 30^\circ$ were considered to minimize multi-path errors.

The degree of *VTEC* disturbance during the period of study was estimated by the deviation from median *VTEC* ($VTEC_{median}$) using equation²⁶:

$$\Delta VTEC = \frac{VTEC - VTEC_{median}}{VTEC_{median}} \times 100 \quad \dots (3)$$

To determine $VTEC_{median}$, the international quietest days published in the Geoscience Australia website http://www.ga.gov.au/oracle/geomag/iqd_form.jsp for the month of February, 2014 were considered. The $\Delta VTEC$ was used to separate perturbation induced changes of TEC from regular behaviour. A positive (negative) $\Delta VTEC$ is a signature of enhancement (depletion) in electron density. The small deviations in *VTEC* ($\pm 20\%$) were considered to be due to day-to-day variability in the ionosphere⁴⁰ and could result due to DD effect, zonal wind effect or local gravity waves generated during thunderstorms or by local heating effects¹⁴. As these changes in *VTEC* may or may not have the effect of a geomagnetic storm, we do not discuss the small *VTEC* deviation in this paper.

Table 1 — IGS stations used in this study

Station (Code)	Geog. Lat (°)	Geog. Lon (°)	Mag. Lat (°)	LT (HH:MM)
Libreville (NKLK)	0.35	9.67	-8.05	UT+0:38
Mbarara (MBAR)	-0.60	30.74	-10.22	UT+2:00
Eldoret (MOIU)	0.29	35.29	-8.10	UT+0:35
Malindi (MAL2)	-2.99	40.19	-11.17	UT+2:40
Seychelles Island (SEY1)	-4.67	55.48	-12.88	UT+3:42

Furthermore, the occurrence of ionospheric irregularities during the period of study was investigated using the rate of change of TEC (ROT). This was computed using the equation^{19,41}:

$$ROT = \frac{VTEC_k^i - VTEC_{k-1}^i}{t_k^i - t_{k-1}^i} \quad \dots (4)$$

where, i is the visible satellite and k is the time of epoch. $VTEC_k^i$ and $VTEC_{k-1}^i$ are consecutive $VTEC$ values at epochs t_k^i and t_{k-1}^i , corresponding to observed satellite i . The ROT can provide information on the spatial variation of the density of electrons in the ionosphere⁴². At low and mid-latitudes, for high elevation angles, the fluctuations in ROT are due to ionospheric irregularities with scale-sizes of several hundred meters to about 2.5 km⁴¹. To quantify the degree of small scale ionospheric irregularities, standard deviation of ROT (Rate of Change of TEC Index, $ROTI$) over a 5 minute interval was obtained⁴¹. Averaging over 5 minute interval allows a relatively high time resolution⁴¹. Any $ROTI$ value ≤ 0.5 TECU/min was considered as background (noise) ionospheric level^{43,44}. The results of this study are presented in the following section.

4 Results and Discussion

4.1 Solar wind and Geophysical conditions

The solar wind parameters and geomagnetic indices associated with this period are presented in Fig. 2. The figure presents variations of V_p , T_p , P , IMF Bz as well as AE, Kp and Dst indices in panels (a)-(g), respectively as functions of Universal Time (UT). In order to trace the events by day, the dates are indicated on top of Fig. 2. Each geomagnetic storm period of interest is highlighted in gray and Sudden Storm commencements (SSC) are indicated with dashed vertical red lines. The UT when the geomagnetic storms attained least Dst value are indicated by red arrows. The blue dotted horizontal lines in panels (d) and (g) indicate the zero mark for IMF Bz and Dst. The following subsections present discussions of each geomagnetic storm.

4.1.1 Storm of 19 February 2014

There was an increase in V_p , T_p , and P which were observed at around 06:00 UT on 18 February 2014, an indication of the arrival of a shock wave. The V_p increased progressively, indicating signatures of a high speed solar wind and it attained the maximum

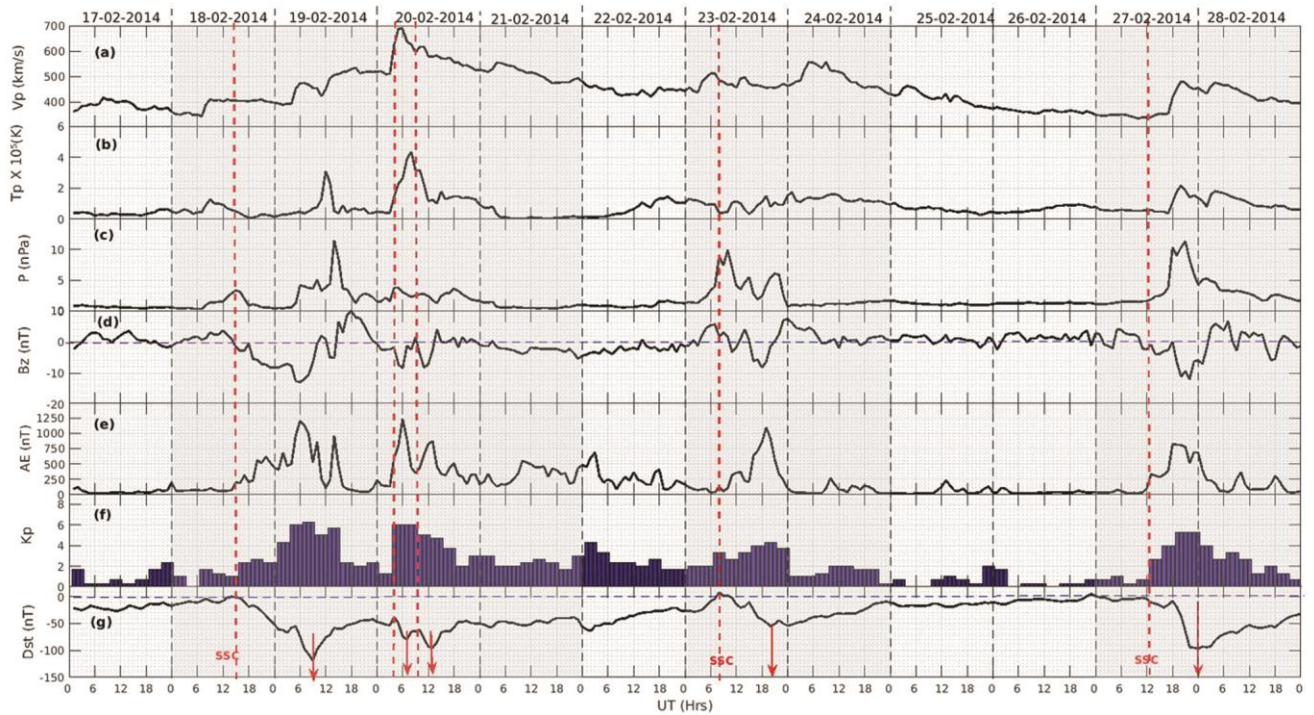


Fig. 2 — The variation of (a) proton speed (V_p), (b) proton temperature (T_p), (c) solar wind speed (P), (d) z - component of IMF (B_z), (e) AE index, (f) Kp and (g) Dst indices as functions of UT during 17-28 February 2014. Each geomagnetic storm period of interest are highlighted in gray and SSCs are indicated with red arrows. The dotted blue horizontal lines in panels (d) and (g) indicate the zero mark for IMF Bz and Dst.

of about 700 km on 20 February 2014. The trend seen on V_p may imply that the geomagnetic storm was preceded by a shock which was almost consistent during the main phase of the storm. The Bz turned south at 06:00 UT on 18 February 2014 following the increase in V_p and reached a minimum of about -14 nT at around 05:00 UT on 19 February 2014. This implies that there may have been a transfer of energy, mass and momentum from the solar wind flow to the magnetosphere through the magnetic reconnection process⁴⁵. The AE index increased from about 100nT following the southward turning of Bz at about 12:00 UT on 18 February 2014 and reached the maximum value of ≈ 1250 nT on 19 February 2014 at around 06:00 UT, indicating that the magnetosphere-ionosphere coupling process at the poles was intense⁴⁶. Panel (g) of Fig. 2 shows SSC at around 12:00 UT on 18 February 2014. The SSC was followed by a decrease in Dst indicating the main phase of the storm and it reached a minimum of ≈ 112 nT at about 09:00 UT on 19 February 2014, while Kp reached the maximum of 6. The decrease in Dst index is caused by an enhancement of the trapped particle population in the magnetosphere and thus by proton ring current flowing westward^{36,47-49}. The storm then entered a recovery phase after 09:00 UT on 19 February 2014, marked by an increase in Dst value.

4.1.2 Storm of 20th February 2014

During the recovery phase of the geomagnetic storm that was triggered on 18 February 2014, a second depression in Dst started at around 03:00 UT on 20 February 2014 and this was accompanied by an increase in the other solar and geomagnetic parameters. An observation of interest was that the Dst index showed a double depression on 20 February 2014 with a minimum of -60 nT at around 06:00 UT and -90 nT at around 13:00 UT, respectively. The double peak signature was also observed on the T_p , P , Bz, AE, and Kp in panels (b)-(f). This event can be categorized as a double step storm e.g.⁴⁷. This may result from the superposition of two successive storms driven by two successive southward IMF Bz⁴⁷. Another reason could be that intense storms can result from two-step development in the ring current, which is initially the result of large-scale convection in the magnetosphere, and eventually sub storm associated injection of ionospheric O⁺ ions into the inner magnetosphere^{50,51}.

4.1.3 Storm of 23 February, 2014

An increase in V_p and T_p was observed on 23 February 2014 at around 00:00 UT, indicating the arrival of a shock wave. They attained the maximum values of ≈ 500 km/s and $\approx 1.0 \times 10^5$ K respectively at around 06:00 UT on 23 February 2014. The Bz turned south and attained a minimum of about -8nT at 18:00 UT, while AE increased, reaching a maximum of ≈ 1100 nT. A SSC was observed at around 05:00 UT on the same day following the southward turning of Bz. The storm then entered a main phase at around 11:00 UT characterised by a decrease in Dst which reached a minimum of about -59nT at 18:00 UT, while Kp attained a maximum value of 4. After 18:00 UT, the storm entered a long duration recovery phase which lasted for the whole of 24 February 2014.

4.1.4 Storm of 27 February, 2014

The solar wind parameters and geomagnetic indices also indicated a disturbance during the evening hours of 27 February 2014. There was an increase in V_p and T_p at around 17:00 UT on 27 February 2014 indicating the arrival of the shock wave and they attained the maximum values of ≈ 500 km/s and $\approx 1.8 \times 10^5$ K, respectively, at around 19:00 UT on 27 February 2014. The Bz turned south to a minimum of about -14nT following the increase in V_p and T_p . This was followed by an increment in AE index at around 12:00 UT and it reached a maximum of about 800nT at around 17:00 UT on 27 February 2014. A SSC occurred at around 12:00 UT on 27 February 2014, and a minimum in Dst of about -99 nT occurred at around 00:00 UT. The three hourly Kp value reached a maximum of 5 at 00:00 UT when Dst was at its minimum value. The effects of the storms on the ionosphere are discussed in terms of the VTEC response in the following subsection.

4.2 VTEC response to the storms

The low latitude ionospheric TEC response to the geomagnetic storms described earlier are presented here. The results include variations in VTEC and VTEC perturbation ($\Delta VTEC$). The diurnal variation of VTEC for each day during the period of study is presented in Fig. 3 over each IGS receiver. Geomagnetic storm days of interest are indicated with a gray background.

It is important to note that the Local Time (LT) is different over these stations and the conversion between UT and LT can be done using the information provided in Table 1. The diurnal pattern of VTEC

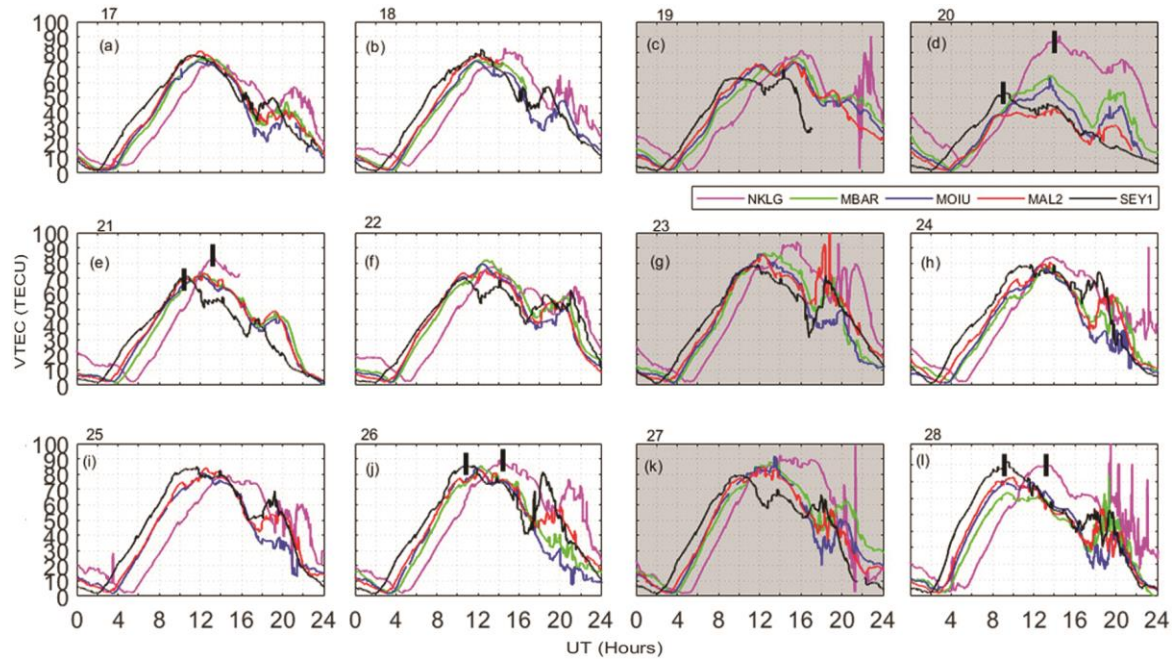


Fig. 3 — Diurnal variation of VTEC over each IGS receiver (see legend) during the period of study. Storm days are identified by a gray background.

showed a steady increase from about sunrise to an afternoon maximum when the Sun was overhead and then fell to a minimum just before sunset over all the IGS receivers. However, the $VTEC$ variations were observed to be much more irregular during the storm days. The peak of $VTEC$ was observed to undergo a time shift from SEY1 to NKLG (examples of which are indicated by black vertical bars in panels (d), (e), (j), (l) for NKLG and SEY1). A similar observation was made for the geomagnetic storm of 15 May 2005 by⁴⁶ over stations at three different longitudes near the Equatorial Ionization Anomaly. Therefore, the features of the storm development depend on the Local Time (LT) of a station.

The result of the derived $VTEC$ and median $VTEC$ (black dotted curve) from the IGS receivers are presented in Fig. 4 as functions of UT. Panel (f) of Fig. 4 shows the Dst index variation during the period of study.

The red arrows in Fig. 4 indicate the approximate UT when minimum Dst was attained during the geomagnetic storm days of interest. On 19 February 2014, the $VTEC$ was greater than monthly median $VTEC$ over most stations after 15:00 UT with a maximum in the range of about 60-80 TECU except over SEY1 (panel (e)). On this day, minimum Dst of about -112 nT was attained at around 08:00 UT as seen from the last panel. Deviations between $VTEC$

and the monthly median $VTEC$ were quantified by the percentage deviations which are presented in Fig. 5. In general, the deviation increased from MAL2 with maximum $\approx 60\%$ to NKLG with maximum $\approx 180\%$ after 18:00 UT. No conclusion can be drawn on the deviation in SEY1 due to the data gap. The increase from MAL2 to NKLG shows a longitudinal dependence on the ionospheric response to geomagnetic storms. The positive percentage deviation over the stations implies a positive ionospheric storm effect on 19 February 2014. This effect was observed several hours after the onset of main phase of the storm (see lower panel of Fig. 5) and southward turning of IMF B_z on 19 February 2014.

Such delayed positive ionospheric storms were also observed by⁵², who studied the variability in the ionosphere during geomagnetic storms over the period 2004-2005. The delayed positive ionospheric storm may be attributed to changes in neutral gas composition^{40,53}. The storm induced circulation transports air rich in atomic oxygen from higher latitudes towards low latitudes, enriching molecular N_2 at mid-latitudes. The enhanced oxygen density affects the ionization process, thus producing the delayed positive storm effects⁵⁴.

The increase in $VTEC$ on 19 February 2014 was followed by $VTEC$ depletion on 20 February 2014

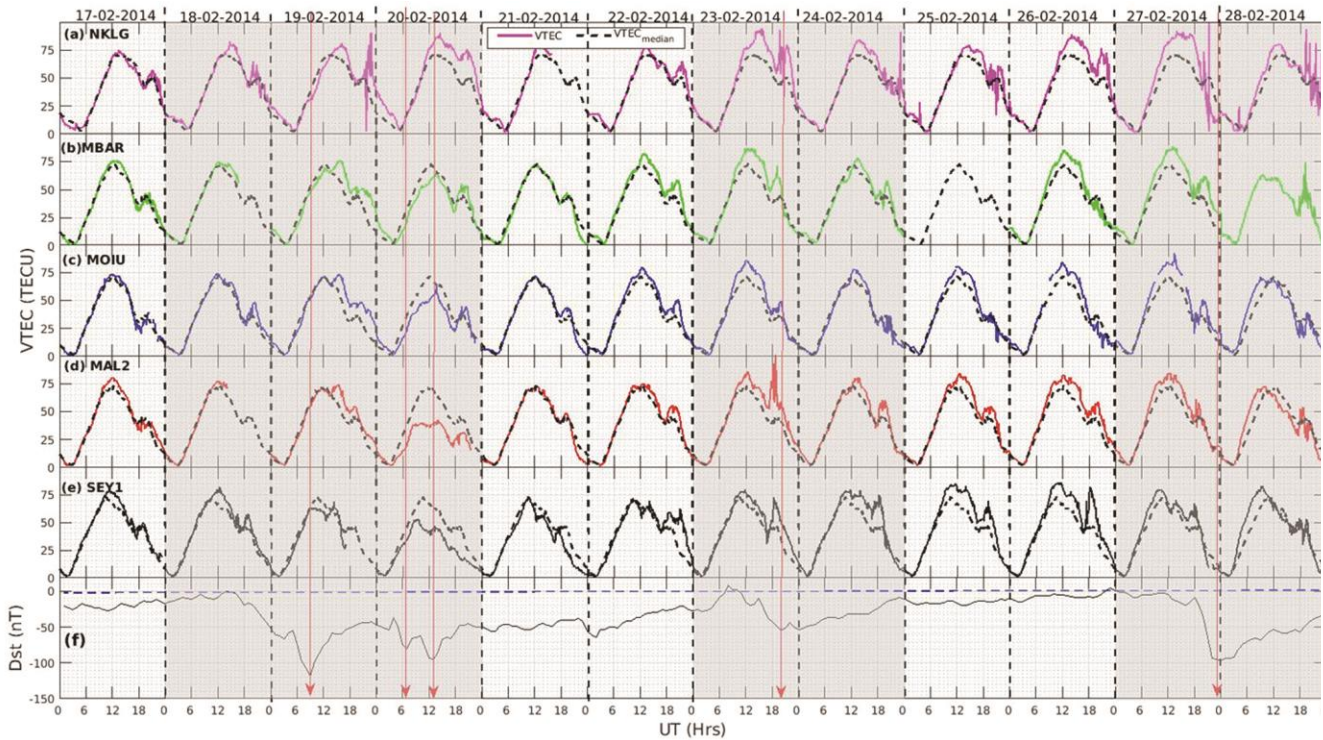


Fig. 4 — VTEC (solid curve) and monthly median VTEC (dotted curve) variations over (a) NKLG, (b) MBAR, (c) MOIU, (d) MAL2, and (e) SEY1 as a function of UT during 17 - 28 February 2014. The storm days are indicated by gray background.

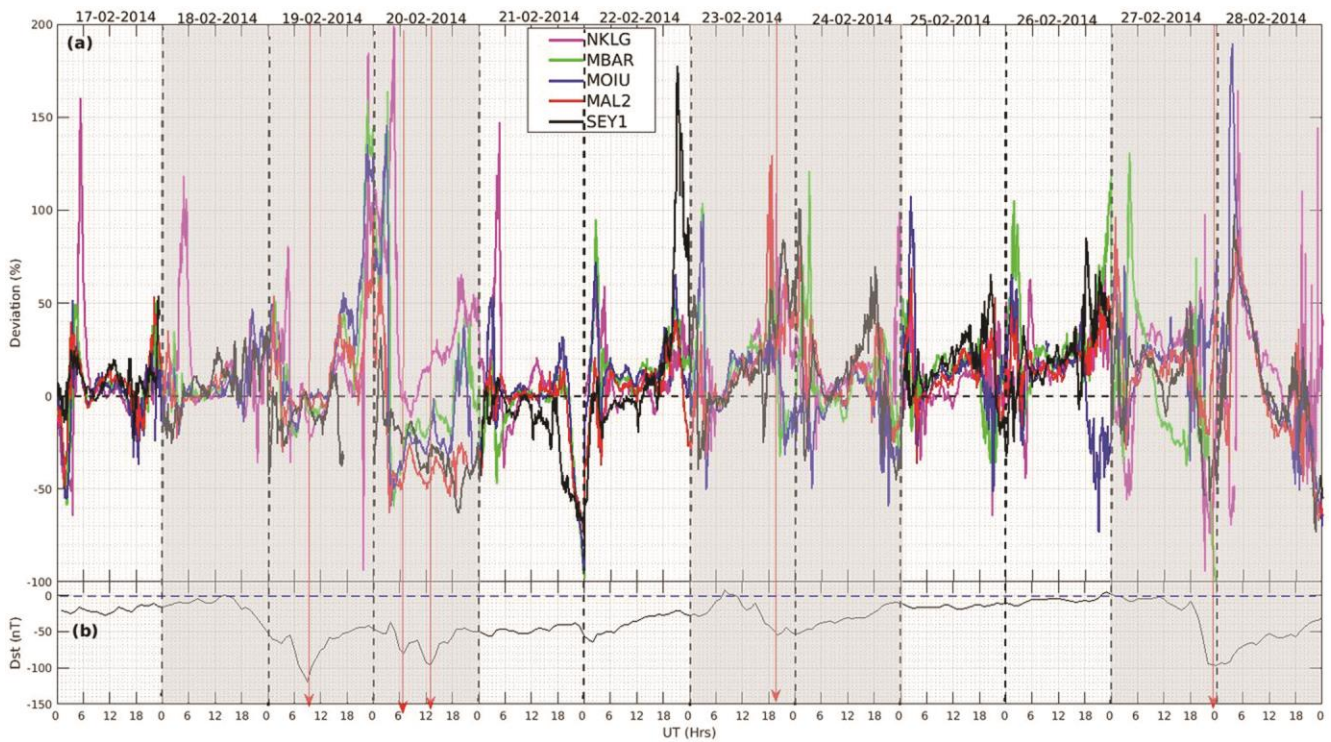


Fig. 5 — Percentage deviation of VTEC over NKLG, MBAR, MOIU, MAL2, and SEY1 for the geomagnetic storm period from 17 - 28 February, 2014. The Dst index is also plotted in panel (b).

over most stations between 06:00 UT and 00:00 UT, with maximum values of about 50 TECU, 45 TECU, 60 TECU, 60 TECU over SEY1, MAL2, MOIU and MBAR, respectively, except over NKLG (panel (a)) where $VTEC$ was greater than monthly median $VTEC$ after 12:00 UT with maximum value of 90 TECU. The percentage deviation was observed to be about -50% over SEY1 and MAL2, -25% over MOIU and MBAR between 06:00 UT and 18:00 UT. However, a deviation of about 50% is observed over NKLG (panel(a)) at around 18:00 UT. A similar negative ionospheric storm effect was observed by²⁶. The negative ionospheric storm effects may be attributed to the Disturbance Dynamo (DD) electric fields^{26,55}, which was associated with enhanced energy deposition into the high latitude ionosphere during geomagnetically active periods²¹. The increase in AE index (see Fig. 2, panel (c)) is an indicator of high energy deposition in the high latitude ionosphere. The production of DD electric fields was due to the increased corpuscular radiation and consequent Joule heating of the high latitude plasma. This additional heating may launch winds towards the equator, which in turn generate the DD electric fields^{3,21}. The energy input to the thermosphere during geomagnetic disturbances alters the global thermospheric circulation and consequently alters the generation of electric fields and currents at middle and low latitudes by ionospheric wind dynamo action²¹.

On 23 February 2014, $VTEC$ was observed to be greater than monthly median $VTEC$ from about 10:00 UT to about 18:00 UT over all the stations. At this time interval, the $VTEC$ reached the maximum values of about 80 TECU, 80 TECU, 85 TECU, 90 TECU and 95 TECU over SEY1, MAL2, MOIU, MBAR and NKLG respectively. On 23 February 2014, the deviation over all stations was between 15% and 25% in the time interval 10:00-18:00 UT. There was a time lag of approximately one hour between the storm main phase commencement and enhancement in $VTEC$ over all stations. As is expected, local uplifting of plasma and its redistribution due to the eastward Prompt Penetration Electric Field (PPEF) would have a certain time constant (\sim an hour or so) and has been observed by^{55,56} etc. Therefore, observation of enhancement in $VTEC$ at almost the same time over all the stations with nearly same magnetic latitude points to a common mechanism (i.e, PPEF) for its formation. This result also implies that the day-time PPEF penetrates almost simultaneously over a wide longitude zone.

On 27 February 2014, $VTEC$ was greater than the monthly median $VTEC$ from 03:00 UT to about 12:00 UT over all the stations. At around 09:00 UT, the maximum $VTEC$ was in the range of 60 and 85 TECU over all the stations. On 28 February 2014, the deviation was about 75% over SEY1, MAL2 and NKLG, 175% over MOIU and 125% over MBAR, an indication of a positive ionospheric storm effect over all the stations. The effect occurred during the recovery phase of the geomagnetic storm which was triggered on 27 February and this may be understood in terms of storm induced wind-lifting effect^{14,22,57}. The energy transfer from the solar wind to the ionosphere involved heating of the auroral regions through particle precipitations and dissipation of ionospheric currents. The auroral heating then intensified thermospheric neutral winds towards the equator. Once the thermospheric winds reached low latitudes, they act to push ionospheric plasma to higher altitudes where recombination rates are low⁵⁸.

In addition, Figs 4 and 5 shows a consistent increase in $VTEC$ from SEY1 to NKLG irrespective of the storm day. The same observation was also made⁵⁹ who presented the occurrence patterns of ionospheric irregularities during quiet geomagnetic conditions over the African low latitude region. The increase of $VTEC$ from SEY1 to NKLG might have been due to the different local times and latitudes of these stations⁵⁹. In addition, we also checked the effect of composition changes during the study period using the [O]/[N₂] ratio from the Global Ultra Violet Imager (GUVI) instrument on-board the Thermosphere Ionosphere Mesosphere Energetics and Dynamics (TIMED) satellite. In this study, we have used the image gallery obtained from <http://guvi.jhuapl.edu/site/gallery/guvi-gallery13on2.shtml> to see the variations of [O]/[N₂] ratio e.g.²⁸. Figure 6 presents the global maps [O]/[N₂] ratio for the study period.

The [O]/[N₂] maps corresponding to the geomagnetic storm days of interest are indicated with black background in Fig. 6. The white spaces in each panel of Fig. 6 indicate data gaps. Figure 6 shows low thermospheric [O]/[N₂] ratio in the eastern part of Africa. The [O]/[N₂] ratio was moderate in Central Africa, while West Africa showed the highest thermospheric [O]/[N₂] ratio. The consistent increase in $VTEC$ from East Africa to West Africa could have been due to large scale wind circulation which led to equatorial composition changes and the increase in [O]/[N₂] ratio⁶⁰. The generation or

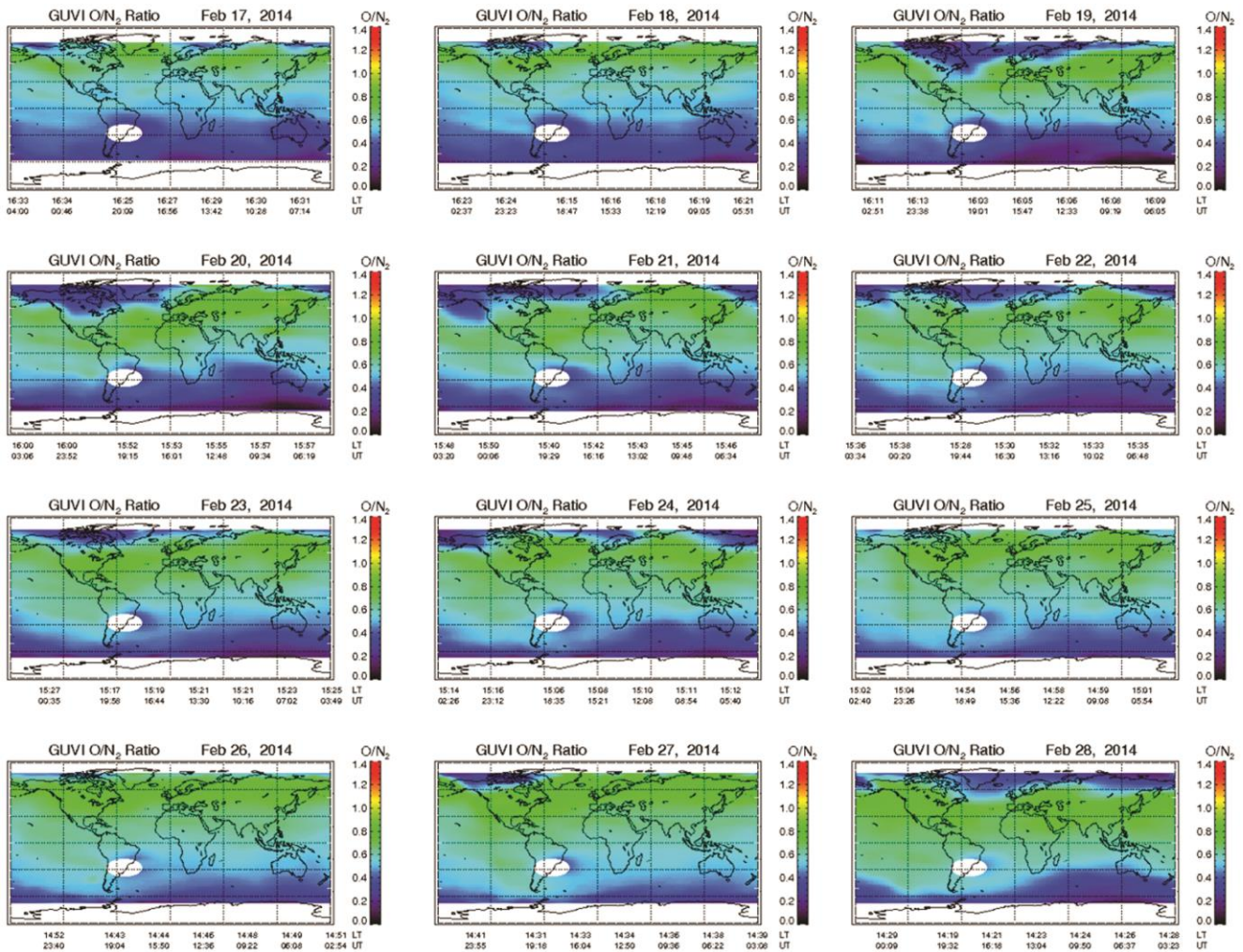


Fig. 6 — Global map of the $[O]/[N_2]$ ratio from the Global Ultraviolet Imager (GUVI) experiment flown on the TIMED satellite for the period from 17-28 February 2014. The geomagnetic storm days of interest are indicated with black background. The white spaces in each panel indicate data gaps.

inhibition of ionospheric irregularities can change drastically during geomagnetic storm activity as presented in the following subsection.

4.3 Occurrence of Ionospheric irregularities

In this section, the occurrences of ionospheric irregularities during the geomagnetic activities are presented. The results include ROTI analysis at 5 minutes interval. The variation of ROTI as a function of UT over NKLG, MBAR, MOIU, MAL2 and SEY1 are represented in Fig. 7 from panels (a)-(e), respectively. The Dst index is also plotted in the bottom panel of Fig. 7. The storm days are indicated by grey background.

Ionospheric irregularities were inhibited over MBAR, MOIU, MAL2 and SEY 1 on 19 February 2014. On the contrary, irregularities were observed

over NKLG between 18:00 UT and 00:00 UT (19:00 LT - 01:00 LT) (maximum ROTI of about 1.5 TECU/min) on 19 February 2014. A storm can generate or inhibit ionospheric irregularities occurrence, depending on the changes in the ring current i.e., Dst index¹⁹. A minimum Dst index of -112nT occurred at around 09:00 UT on 19 February 2014 (corresponding to 13:00 LT in SEY1, 12:00 LT in MBAR, MOIU and MAL2, 10:00 LT in NKLG). These were categorized as early afternoon hours over the stations¹⁹. If the maximum negative Dst index, occurs in the early afternoon, irregularities would be inhibited¹⁹. During the early afternoon hours, the eastward PPEF was increased, causing an increase in F-layer height. A negative excursion of ring current during this period may lower the local eastward electric field and reduce the

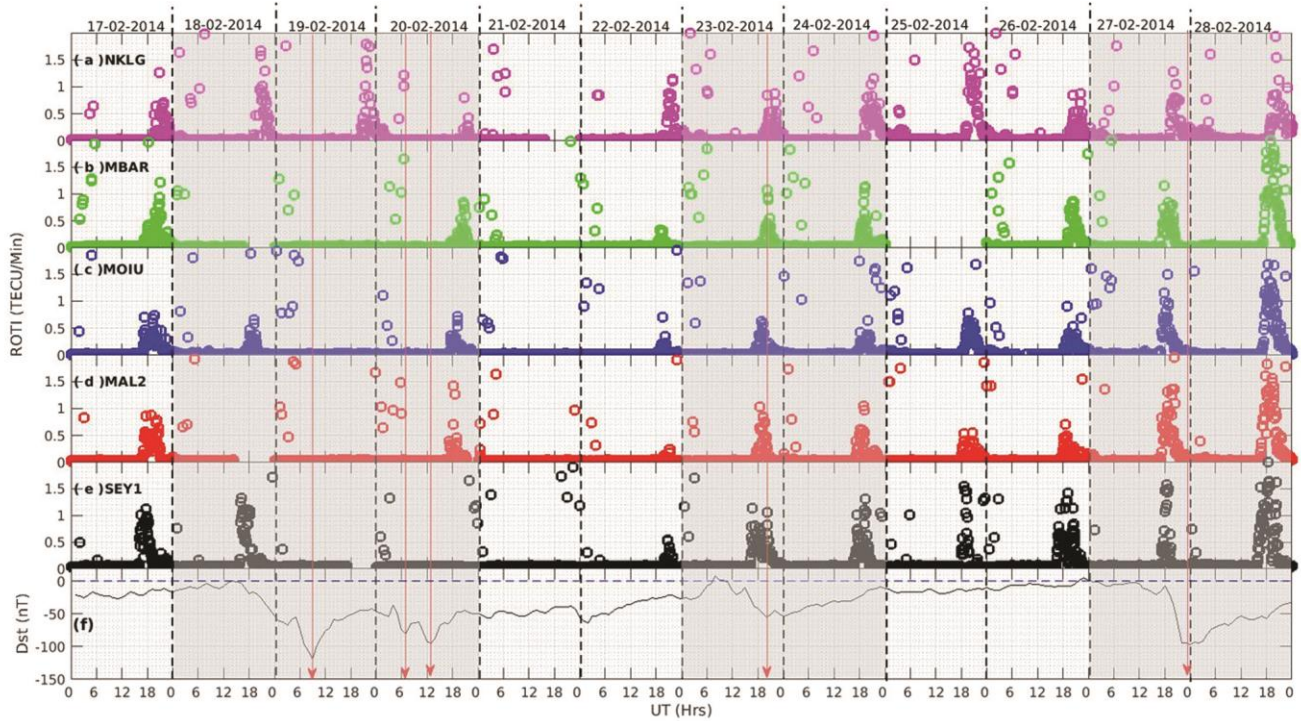


Fig. 7 — Variation of ROTI as a function of UT over (a) NKLK, (b) MBAR, (c) MOIU, (d) MAL2 and (e) SEY1 for the period from 17 - 28 February 2014. The storm days are indicated by grey background.

F-layer height. This effect may sometimes be large enough to reverse the upward movement of F-layer plasma during the post sunset period, thereby inhibiting the creation of irregularities¹⁹.

On 20 February 2014, ROTI values were 0.5 TECU/Min on average over MAL2, MOIU, MBAR and NKLK, while no increment in ROTI was observed over SEY1. Hence, irregularities were inhibited over all stations on 20 February 2014. The occurrence of the irregularities as determined by higher values of ROTI corresponds to the period of depletion in VTEC (see Fig. 5). As mentioned earlier, the VTEC depletion on 20 February 2014 was attributed to DD electric fields. The DD westward zonal electric fields reached low latitudes and reduced the plasma upward drift during the day and downward drift during the night. In this way, the pre-reversal vertical drift peak was reduced in amplitude and as a result, the ionospheric irregularity generation was inhibited. In addition, shifts in the peaks of ROTI were observed to occur from one station to another, confirming a LT and longitude dependence of the occurrence of ionospheric irregularities⁶¹.

On 23 February 2014, ROTI values were ~ 1 TECU/Min over SEY1, MAL2, MBAR and NKLK and ~ 0.75 TECU/Min over MOIU between 18:00 UT

and 0:00 UT. This is an indication that irregularities were triggered over all the stations on 23 February 2014. The Minimum Dst of about -60nT occurred at around 00:00 UT (see Fig. 2). This corresponds to 04:00 LT in SEY1, 03:00 LT in MBAR, MOIU and MAL2 and 01:00 LT in NKLK. This corresponds to midnight-postmidnight time and irregularities were observed in all the stations. The possible explanation for the occurrence of irregularities after the sunset is primarily the Rayleigh-Taylor plasma instability mechanism¹⁹. After the sunset and along the dip equator, the ionospheric plasma was uplifted, where the electric field during the day-time was mapped from the E-region to the F-region. The zonal electric field in the equatorial ionosphere was eastward during the day-time. Immediately after the sunset, this eastward electric field was enhanced due to conductivity gradient at the terminator, a process called the pre-reversal enhancement¹⁹. The plasma from the F-region at the dip equator is then uplifted to higher altitudes, and at the same time the plasma in the E-region quickly diminished due to the decreasing intensity of solar radiation.

On 28 February 2014, ROTI values were ≈ 2.5 TECU/Min over SEY1 and MBAR, 2 TECU/Min over MAL2 and NKLK and 1.5 TECU/Min over MOIU

between about 18:00 UT and 0:00 UT. Therefore, irregularities occurred over all the stations after the sunset just as that of 23 February 2014. The intensity of the irregularity was seen to increase from SEY1 to NKLG. Minimum Dst (-99nT) occurred at 00:00 UT (04:00 LT in SEY1, 03:00 LT in MBAR, MOIU and MAL2, 01:00 LT in NKLG) corresponding to midnight-postmidnight time period^{19,45}. Generation of irregularities could have also been due to the Rayleigh-Taylor plasma instability mechanisms as described for 23 February 2014.

5 Conclusions

This study focused on the effects of space weather on the ionosphere during geomagnetic storms for the period from 17-28 February 2014 over African low latitude region. A total of four geomagnetic storms were identified within this period. By inspecting the Dst index it was revealed that the storms on 19, 23 and 27 February, 2014 were preceded by SSC and they attained minimum Dst values of -112 nT on 19 February 2014, -59 nT on 23 February 2014 and -99 nT on 27 February 2014, respectively. The geomagnetic storm on 20 February 2014 was categorized as a double step storm because the Dst index showed a double minimum signature which was also observable in most of the other solar and geophysical parameters.

The ionospheric response to the geomagnetic storms which occurred during the study period showed both negative and positive storm effects. In particular, the geomagnetic storm on 19 February 2014, caused a delayed positive storm effect. This was attributed to changes in neutral gas composition. The event on 20 February 2014 caused a negative ionospheric storm effect. The DD electric fields may have led to the negative ionospheric storm over all the stations considered. On 23 February 2014, a positive ionospheric storm was observed. Maximum VTEC occurred after about an hour of SSC. This was attributed to PPEF. On 28 February 2014, a positive ionospheric storm effect was observed in the early morning hours, during the recovery phase of the storm which was triggered on 27 February 2014. This was explained in terms of storm induced wind-lifting effect. The only identified factor is that the pronounced double step storm on 20 February 2014 caused a negative ionospheric storm, while the rest of the storms caused a positive effect. Furthermore, a longitudinal dependence on the ionospheric response

to the geomagnetic storms was observed. A consistent increase in VTEC from SEY1 to NKLG was observed in all the geomagnetic storm days. This was attributed to large scale wind circulation which led to equatorial composition changes.

Out of all the storms studied, the storms on 19 and 20 February 2014, inhibited the occurrence of ionospheric irregularities, while the remaining storms triggered ionospheric irregularities. In particular, the weakening of the ionospheric irregularity on 20 February 2014 was attributed to the DD electric field. Ionospheric irregularities were inhibited over most IGS stations on 19 February 2014. The maximum negative Dst index occurred in the afternoon hours on 19 February 2014. If the maximum negative Dst index, occurs in the early afternoon, irregularities would be inhibited. Generation of irregularities on 23 and 27 February 2014 may have been due to the Rayleigh-Taylor plasma instability.

Acknowledgements

The authors would like to acknowledge the financial support offered by the International Science program of Sweden (code UGA: 02) towards this study. The data used in this study were obtained from <http://www.kugi.kyoto-u.ac.jp> and <http://www.srl.caltech.edu/ACE/ASC/>. In addition, the international GNSS service (IGS) is acknowledged for providing the GPS data.

References

- 1 Gonzalez W, Joselyn J, Kamide Y, Kroehl H, Rostoker G, Tsurutani B and Vasyliunas V, *Journal of Geophysical Research: Space Physics*, 99(A4) (1994) 5771.
- 2 Kelley M, ser. *International Geophysics*, Elsevier, 43 (2009).
- 3 Dashora N & Pandey R, *Earth, Planets, and Space*, 59 (2007) 127.
- 4 Gonzalez W D, Clúa de Gonzalez A L, Sobral J H A, Dal Lago A & Vieira L E, *Journal of Atmospheric and Solar-Terrestrial Physics*, 63 (2001) 403.
- 5 Zhang J, Liemohn M W, Kozyra J U, Thomsen M F, Elliott H A & Weygand J M, *Journal of Geophysical Research (Space Physics)*, 111 (2006) A01104.
- 6 Jones K L, *Journal of Atmospheric and Terrestrial Physics*, 33 (1971) 379.
- 7 Jones K L & Rishbeth H, *Journal of Atmospheric and Terrestrial Physics*, 33 (1971) 391.
- 8 Volland H, *Journal of Atmospheric and Terrestrial Physics*, 41 (1979) 853.
- 9 Mayr H G, Harris I & Spencer N W, *Reviews of Geophysics and Space Physics*, 16 (1978) 539.
- 10 Karan D K & Pallamraju D, *Journal of Atmospheric and Solar-Terrestrial Physics*, 170 (2018) 35.

- 11 Rao P V S Rama, Krishna S Gopi, Prasad J Vara, Prasad S N V S, Prasad D S V V D & Niranjana K, *Annales Geophysicae*, 27 (2009) 2101.
- 12 Ngwira C M, McKinnell L-A, Cilliers P J & Yizengaw E, *Advances in Space Research*, 49 (2012) 327.
- 13 Buonsato M J, *Space Science Review*, 88 (1999) 563.
- 14 Kumar S, Chandra H & Sharma S, *Journal of Atmospheric and Solar-Terrestrial Physics*, 67 (2005) 581.
- 15 Fejer B G & Scherliess L, *Geophysical Research Letters*, 22 (1995) 851.
- 16 Fejer B G, *Journal of Atmospheric and Solar-Terrestrial Physics*, 64 (2002) 1401.
- 17 Scherliess L & Fejer B G, *Journal of Geophysical Research*, 102 (1997) 24037.
- 18 Zhao B, Wan W, Liu L, Igarashi K, Yumoto K & Ning B, *Journal of Atmospheric and Solar-Terrestrial Physics*, 71 (2009) 88.
- 19 Aarons J, *Radio Science*, 26 (1991) 1131.
- 20 De Rezende L F C d, Paula E R d, Batista I S, Kantor I J & Muella M T d A H, *Revista Brasileira de Geofísica*, 25 (2007) 151.
- 21 Blanc M & Richmond A D, *Journal of Geophysical Research*, 85 (1980) 1669.
- 22 Kumar S & Singh A K, *Advances in Space Research*, 47 (2010) 710.
- 23 Ho C M, Mannucci A J, Lindqwister U J, Pi X & Tsurutani B T, *Geophysical Research Letters*, 23 (1996) 3219.
- 24 Jakowski N, Schlüter S & Sardon E, *Journal of Atmospheric and Solar-Terrestrial Physics*, 61 (1999) 299.
- 25 Jain A, Tiwari A, Jain S & Gwal A K, *Indian J Radio Space Phys*, 39 (2010) 11.
- 26 Adewale A O, Oyeyemi E O, Adeloye A B, Ngwira C M & Athieno R, *Journal of Geophysical Research (Space Physics)*, 116 (2011) A12319.
- 27 Habarulema J B, McKinnell L-A, Burešová D, Zhang Y, Seemala G, Ngwira C, Chum J, & Opperman B, *Journal of Atmospheric and Solar-Terrestrial Physics*, 102 (2013) 105.
- 28 Tesema F, Dantie B & Nigusie M, *Journal of Atmospheric and Solar-Terrestrial Physics*, 135 (2015) 143.
- 29 Ghamry E, Lethy A, Arafa-Hamed T & Abd Elaal E, *NRIAG Journal of Astronomy and Geophysics*, 5 (2016) 263.
- 30 Khalifa M, Benkhaldoun Z, Vilmer N, Bounhir A, Makela J J, Kaab M & Lagheryeb A, *IAU General Assembly*, 22 (2015) 2251685.
- 31 Kurkin V I, Polekh N M, Ponomarchuk S N, Podlesny A V, Zolotukhina N A & Romanova E B, *PIERS Proceedings, Prague, Czech Republic, July 69*, 5 (2015) 263.
- 32 Zakharenkova I, Astafyeva E and Cherniak I, *Journal of Geophysical Research (Space Physics)*, 120 (2015) 8817.
- 33 Pirog O M, Polekh N M, Zherebtsov G A, Smirnov V F, Shi J K & Wang X, *Advances in Space Research*, 37 (2006) 1075.
- 34 Dashora N, Sharma S, Dabas R S, Alex S & Pandey R, *Annales Geophysicae*, 27 (2009) 1803.
- 35 Davis T N & Sugiura M, *Journal of Geophysical Research*, 71 (1966) 785.
- 36 Rostoker G, *Reviews of Geophysics and Space Physics*, 10 (1972) 935.
- 37 Seemala G K & Valladares C E, *Radio Science*, 46 (2011) 5019.
- 38 Rama Rao P V S, Gopi Krishna S, Niranjana K & Prasad D S V V D, *Annales Geophysicae*, 24 (2006) 3279.
- 39 Hofmann-Wellenhof B, Lichtenegger H & Collins J, *Theory and practice*, (1992).
- 40 Rishbeth H, F-region storms and thermospheric circulation. In Sandholt, P. E. and Egeland, A., editors, *Electromagnetic Coupling in the Polar Clefts and Caps*, (1989) 393.
- 41 Pi X, Mannucci A J, Lindqwister U J, & Ho C M, *Geophysical Research Letters*, 24 (1997) 2283.
- 42 Basu S, Groves K M, Quinn J M & Doherty P, *Journal of Atmospheric and Solar-Terrestrial Physics*, 61 (1999) 1219.
- 43 Ma G & Maruyama T, *Annales Geophysicae*, 21 (2003) 2083.
- 44 Tanna H J, Karia S P, & Pathak K N, *Advances in Space Research*, 52 (2013) 412.
- 45 Oladipo O A & Schüler T, *Journal of Atmospheric and Solar-Terrestrial Physics*, 92 (2013) 78.
- 46 Sharma S, Galav P, Dashora N and Pandey R, *Annales Geophysicae*, 29 (2011) 1063.
- 47 Kamide Y, Yokoyama N, Gonzalez W, Tsurutani B T, Daglis I A, Brekke A & Masuda S, *Journal of Geophysical Research*, 103 (1998) 6917.
- 48 Moldwin, M, *An Introduction to Space Weather* (2008).
- 49 Schunk R W & Nagy A F, *Ionospheres: Physics, Plasma Physics and Chemistry Second Edition*, (2009).
- 50 Burton R K, McPherron R L & Russell C T, *Journal of Geophysical Research*, 80 (1975) 4204.
- 51 Daglis I A, *Washington DC American Geophysical Union Geophysical Monograph Series*, 98 (1997) 107.
- 52 Rakhee M, Shivalika S, Shweta M & Gwal A K, *J. Ind. Geophys. Union*, 14 (2010) 47.
- 53 Mendillo M, *Reviews of Geophysics*, 44 (2006) 4001.
- 54 Prölss G W, *Annales Geophysicae*, 11 (1993) 1.
- 55 Bagiya M S, Joshi H P, Iyer K N, Aggarwal M, Ravindran S & Pathan B M, *Annales Geophysicae*, 27 (2009) 1047.
- 56 Tsurutani B, Mannucci A, Iijima B, Abdu M A, Sobral J H A, Gonzalez W, Guarnieri F, Tsuda T, Saito A, Yumoto K, Fejer B, Fuller-Rowell T J, Kozyra J, Foster J C, Coster A & Vasyliunas V M, *Journal of Geophysical Research (Space Physics)*, 109 (2004) A08302.
- 57 Lin C H, Richmond A D, Heelis R A, Bailey G J, Lu G, Liu J Y, Yeh H C & Su S Y, *Journal of Geophysical Research (Space Physics)*, 110 (2005) A12312.
- 58 Pokhotelov D, Mitchell C N, Spencer P S J, Hairston M R & Heelis R A, *Journal of Geophysical Research (Space Physics)*, 113 (2008) A00A16.
- 59 Mungufeni P, Habarulema J B & Jurua E, *Journal of Atmospheric and Solar-Terrestrial Physics*, 138-139 (2016) 261.
- 60 Prölss G W, *Handbook of Atmospheric Electrodynamics*, 2.22 (1995).
- 61 Valladares C, Villalobos J, Sheehan R & Hagan M, *Annales Geophysicae*, 22 (2004) 3155.